Stability and accuracy of active shielding for grounded capacitive sensors

Ferran Reverter[1,2]**, Xiujun Li**[2] **and Gerard C M Meijer**[2]

[1] Castelldefels School of Technology (EPSC), Technical University of Catalonia (UPC),
Avda Canal Olimpic s/n, 08860 Castelldefels, Barcelona, Spain
[2] Electronic Instrumentation Laboratory, Delft University of Technology (TU Delft),
Mekelweg 4, 2628 CD Delft, The Netherlands

E-mail: reverter@eel.upc.edu

Abstract
Active shielding is commonly used to measure remote grounded capacitive
sensors because it reduces the effects of both external noise/interference and
parasitic capacitances of the shielded cable. However, due to active
shielding, the measurement circuit can become unstable and inaccurate. This
paper analyses these limitations theoretically and experimentally, and then
provides guidelines for improving the performance of active shielding. One
of the key points is the selection of the bandwidth of the amplifier that drives
the shield of the coaxial cable. A wide bandwidth improves accuracy, but a
narrow bandwidth improves stability. Therefore, there is a trade-off between
stability and accuracy with respect to the bandwidth of the amplifier.

Keywords: active shielding, capacitive sensor, operational amplifier, stability,
accuracy

(Some figures in this article are in colour only in the electronic version)

1. Introduction

Capacitive sensors are increasingly common in laboratory
and industrial measurements because they can be built with
affordable technologies, can be tailored to the geometry of
different applications and have low power consumption [1].
This paper deals with interface circuits for grounded capacitive
sensors, i.e. sensors in which one of the two electrodes is
connected to the ground. Several humidity sensors, liquid-
level sensors [2, 3] and distance/proximity sensors [4] belong
to this group.

In many industrial applications, the sensor is not close
to its readout circuit. In these cases, to reduce the effects
of external noise and interference, the sensor is connected
to the circuit using a coaxial or shielded cable. There are
two types of shielding: passive and active. In the case of
passive shielding, the outer conductor is connected to the
ground, as shown in figure 1(*a*). Regrettably, this shielding
is not suitable for grounded capacitive sensors because the
parasitic capacitance of the coaxial cable (C_p), whose value
can be much greater than that of the sensor and depends on

the environmental conditions, would be in parallel with the
sensor (C_x) [5].

In the case of active shielding, the outer conductor is
driven at the same potential as that of the inner conductor by
using a buffer amplifier [6, 7], as shown in figure 1(*b*). Here,
on the one hand, external interferences are driven to ground
through the low output impedance of the amplifier and, on
the other hand, C_p ideally does not affect the measurement of
C_x because both cable conductors are at the same potential.
Therefore, in principle, this technique solves the drawbacks of
passive shielding. However, due to the parasitic components of
the coaxial cable, the buffer amplifier has a positive feedback
path that can bring about instability [8–11]. In addition, due
to the limited bandwidth of the buffer amplifier, the inner and
outer conductors of the coaxial cable are not at exactly the same
potential. Consequently, the effect of C_p is not completely
cancelled, thus limiting the accuracy of the measurement.

This paper analyses the stability and accuracy of the active
shielding technique when it is applied in the measurement
of grounded capacitive sensors. This analysis provides
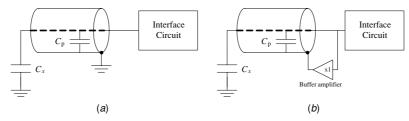guidelines for selecting the bandwidth of the buffer amplifier.

Figure 1. Measurement of a grounded capacitive sensor (C_x) using (*a*) passive shielding and (*b*) active shielding.
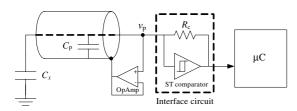

Figure 2. Measurement of a grounded capacitive sensor (C_x) using active shielding and an RC oscillator as an interface circuit.
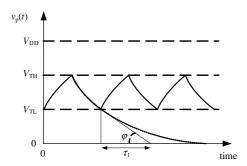

Figure 3. Waveform of the voltage v_p (figure 2) during the charging–discharging process.

2. Circuit overview

Grounded capacitive sensors are usually measured using *RC* oscillator circuits, which can easily be implemented with, for instance, a 555 timer IC [1, 10] or a comparator-based relaxation oscillator [4, 10, 11]. Such an *RC* oscillator basically relies on a Schmitt trigger (ST) comparator, which has an upper (V_{TH}) and a lower (V_{TL}) threshold voltage, a resistor R_c and the capacitive sensor C_x itself, as shown in figure 2. The oscillator circuit works as follows. Let us consider that first the comparator has a high-level output voltage. Then, C_x is charged towards the positive supply voltage (V_{DD}) through R_c and, hence, the voltage v_p increases exponentially with a time constant $\tau_1 = R_c C_x$. When v_p reaches V_{TH}, the comparator is triggered. Afterwards, the comparator has a low-level output voltage and, hence, C_x is discharged towards ground through R_c and v_p decreases exponentially. When v_p reaches V_{TL}, the output of the comparator returns to its initial state and the process starts again. Figure 3 shows the resulting exponential waveform of v_p during the charging–discharging process.

Under ideal conditions, the output of the comparator is a square-wave signal whose period is proportional to C_x [12]. This time-based output signal can be measured directly using a digital system, such as a microcontroller, as shown in figure 2.

The circuit can also include one or more reference capacitors (which are selected by an analogue multiplexer) to compensate for the deviation of the resistor, the supply voltage and the threshold voltages [11].

The function of the buffer amplifier that drives the shield of the coaxial cable can easily be carried out by an operational amplifier (OpAmp) configured as a voltage follower, as shown in figure 2. In order to drive the shield correctly, the OpAmp must (a) be unity-gain stable, (b) have a slew rate greater than the maximal slope of the exponential signal (figure 3) and (c) have a rail-to-rail input/output topology or, at least, the common-mode input voltage range and the output swing must include the voltage range of the exponential signal (figure 3). Regrettably, it is not clear how to select the bandwidth of the OpAmp in order to achieve a good performance. Next, we will provide rules for bandwidth selection.

3. Theoretical analysis

The performance of active shielding is analysed using the circuit shown in figure 4(*a*). This circuit uses an input voltage v_{in} instead of the voltage provided by the ST comparator in figure 2. The voltage to be analysed is v_p, which is the voltage that will then be compared to the threshold voltages of the ST comparator.

Figure 4(*b*) shows the equivalent circuit of figure 4(*a*) when the parasitic components of the interconnection cable are taken into account. The capacitor C_p represents the capacitance between the inner conductor and the shield of the coaxial cable, L_p is the inductance of the current loop between the circuit and C_x, and R_p is the resistance of the interconnection conductors. Let us assume that R_p, C_p and L_p depend linearly on the length ℓ of the interconnection cable and define r_p, c_p as l_p as the parasitic resistance, capacitance and inductance per unit length, respectively.

With regard to the OpAmp, we apply the macro-model shown in figure 5, which includes two voltage-controlled voltage sources (VCVS). The first VCVS has a gain of A_0, which is the differential dc gain of the OpAmp, whereas the second VCVS has a unity gain. The resistor R_{opa} and the capacitor C_{opa} model the frequency limitations. As a result, the OpAmp has a dominant pole $\omega_a = 2\pi f_a = (R_{opa} C_{opa})^{-1}$ and a unity-gain bandwidth $\omega_b = 2\pi f_b = A_0 \omega_a$. The model in figure 5 also takes into account the output resistance R_o.

A voltage follower based on the OpAmp shown in figure 5 behaves as a unity-gain first-order system with a time constant $\tau_b = 1/\omega_b$. If the threshold voltages of the ST comparator are close to each other, then the input signal of the voltage follower shows an almost triangular wave shape, as shown in figure 3. The response of a unity-gain first-order system to a ramp input
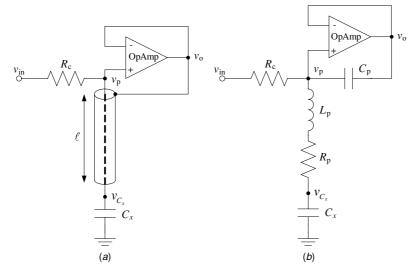
Figure 4. (*a*) Simplified circuit used to analyse the performance of active shielding. (*b*) Equivalent circuit that includes the parasitic components of the interconnection cable.
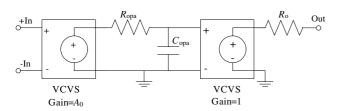

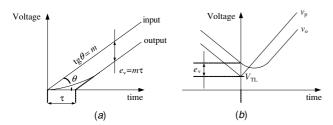**Figure 5.** Macro-model of the OpAmp that considers the dominant-pole open-loop response and the output resistance R_o.

Figure 6. (*a*) Response of a unity-gain first-order system to a ramp input signal. (*b*) Waveforms of the input (v_p) and output (v_o) signals of the voltage follower at the beginning of the charging stage.

signal is shown in figure 6(*a*) [10], where m is the slew rate of the input signal, τ is the time constant of the system and e_v, which is equal to $m\tau$, is the voltage difference between the input and the output. Therefore, the output signal of the voltage follower will differ slightly from the input signal. As an example, figure 6(*b*) shows the input (v_p) and output (v_o) signals of the voltage follower at the beginning of the charging stage.

Taking into account the above models, next we analyse theoretically the stability and accuracy of the circuit.

3.1. Stability

A systematic analysis of the circuit in figure 4(*b*) provides the following fourth-order transfer function between $V_p(s)$ and

$V_{in}(s)$:

$$H(s) = \frac{V_p(s)}{V_{in}(s)} = \frac{Q(s)[(R_oC_ps + 1)(s + \omega_a) + \omega_b]}{P(s)(s + \omega_a) + (Q(s) + R_cC_xs)\omega_b}, \quad (1)$$

where

$$Q(s) = C_xL_ps^2 + R_pC_xs + 1, \quad (2)$$

$$
\begin{aligned}
P(s) = {} & C_pC_xL_p(R_o + R_c)s^3 \\
& + C_x[L_p + C_p(R_oR_p + R_cR_p + R_cR_o)]s^2 \\
& + (R_oC_p + R_pC_x + R_cC_x + R_cC_p)s + 1.
\end{aligned} \quad (3)
$$

If we consider some practical relations between the parameters (e.g. $R_c \gg R_o$, $R_c \gg R_p$, $\omega_b \gg \omega_a$), then the denominator polynomial $d(s)$ of equation (1) is simplified to

$$
\begin{aligned}
d(s) \approx {} & R_cC_pC_xL_ps^4 + R_cC_pC_x(R_p + R_o)s^3 \\
& + [R_c(C_p + C_x) + C_xL_p\omega_b]s^2 + (1 + R_cC_x\omega_b)s + \omega_b.
\end{aligned} \quad (4)
$$

By applying the Routh–Hurwitz stability criterion [13] in equation (4), we obtain the following stability condition:

$$f_b < f_{stab} = \frac{1}{2\pi}\frac{R_c(C_p + C_x)(R_p + R_o) - L_p}{C_xL_p(R_c - R_p - R_o)}, \quad (5)$$

where the frequency f_{stab}, which is determined by the components of the circuit in figure 4(*b*), is defined as the maximal allowable bandwidth of the OpAmp to guarantee stability.

Figure 7 depicts the value of f_{stab} as calculated from equation (5) versus C_x for different lengths of the coaxial cable. We consider $r_p = 1.0 \ \Omega \ m^{-1}$, $c_p = 100 \ pF \ m^{-1}$ and $l_p = 1.0 \ \mu H \ m^{-1}$, which are the features of the interconnection cable used in the experimental setup, and $R_c = 100 \ k\Omega$. The output resistance of an OpAmp generally ranges from 50 Ω to 200 Ω [14]. Here we apply the minimal value (i.e. $R_o = 50 \ \Omega$) since, according to equation (5), this is the worst case in terms of stability. Applying the minimal value of R_o to estimate f_{stab} can bring us to reject an OpAmp that could be used, but this is much better than to accept an OpAmp that makes the circuit unstable. Figure 7 shows that the greater either C_x or ℓ, the
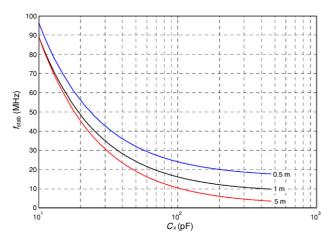
Figure 7. Maximal allowable bandwidth (f_{stab}) of the OpAmp to guarantee stability versus C_x for different lengths of the coaxial cable.

Figure 8. Ideal and actual exponential waveform of v_p during the charging stage.

smaller f_{stab} and, hence, the smaller the maximal allowable bandwidth of the OpAmp. For instance, for $C_x = 100$ pF and $\ell = 1$ m, the circuit is stable when $f_b < 16$ MHz.

Equation (5) shows that practically f_{stab} is inversely proportional to the parasitic inductance L_p. Therefore, we can improve the stability of the circuit by decreasing L_p, i.e. by decreasing the area of the current loop between the circuit and C_x [15]. On the other hand, as either C_p or the factor $R_p + R_o$ increases, so does f_{stab}. Accordingly, a capacitor placed in parallel with C_p and/or a resistor added in series with either R_p or R_o should improve stability.

3.2. Accuracy

Let us first evaluate the circuit in figure 4(a) excluding the buffer amplifier and the coaxial cable, i.e. a simple RC circuit with a time constant $\tau_1 = R_c C_x$. Under these conditions, the voltages v_p and v_{C_x} correspond to the same point. A systematic analysis of this circuit by assuming $v_{C_x}(0) = V_{TL}$ (figure 3) provides, in the Laplace domain,

$$V_p(s) = \frac{1}{s + \omega_1} \left[\omega_1 V_{in}(s) + V_{TL} \right], \qquad (6)$$

where $\omega_1 = 1/\tau_1$. During the charging stage, the input voltage shows a step of magnitude V_{DD}, i.e. $V_{in}(s) = V_{DD}/s$. Then, transforming equation (6) into the time domain yields the following transient response:

$$v_p(t) = V_{DD} + (V_{TL} - V_{DD}) \exp(-\omega_1 t). \qquad (7)$$

From equation (7), the time interval t_{ch} needed to charge C_x through R_c from V_{TL} to V_{TH} equals

$$t_{ch} = \tau_1 \ln \left[\frac{V_{DD} - V_{TL}}{V_{DD} - V_{TH}} \right]. \qquad (8)$$

Let us now analyse the effect of active shielding on the time interval t_{ch}. Firstly, if the stability of the circuit is guaranteed, the inaccuracy can be evaluated by applying a simplified circuit model. In relation to the interconnection cable (figure 4(b)), the effects of L_p and R_p are neglected; the capacitor C_p has a dominant effect on the accuracy, which will be proved experimentally in section 4. With regard to the OpAmp (figure 5), the effect of R_o is also neglected. Secondly,
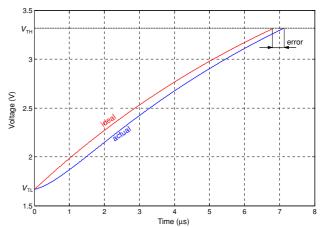
the initial conditions here are $v_{C_x}(0) = V_{TL}$, $v_{C_{opa}}(0) = V_{TL} + e_v$ and $v_{C_p}(0) = -e_v$, where e_v is the voltage difference between the input and the output of the OpAmp due to its limited bandwidth. Just when the discharging signal reaches V_{TL}, the slew rate is $m = \tan \varphi = V_{TL}/\tau_1$ (figure 3) and, hence, the voltage error is $e_v = (\omega_1/\omega_b) V_{TL}$ (figure 6(b)). Taking into account the above considerations, the initial conditions and $\omega_b \gg \omega_a$, we find, in the Laplace domain,

$$V_p(s) \approx \frac{1}{G(s)} [(s + \omega_b) V_{in}(s) + s R_c (C_p + C_x) V_{TL} \\ + \omega_b R_c (V_{TL} C_x - e_v C_p)], \qquad (9)$$

where

$$G(s) = s^2 R_c (C_p + C_x) + s(1 + \omega_b R_c C_x) + \omega_b. \qquad (10)$$

Then, for $V_{in}(s) = V_{DD}/s$, transforming equation (9) into the time domain yields

$$v_p(t) = \left(\frac{k_1}{s_1 - s_2} + \frac{k_2 + V_{TL} s_1^2}{(s_1 - s_2) s_1} \right) \exp(s_1 t) \\ - \left(\frac{k_1}{s_1 - s_2} + \frac{k_2 + V_{TL} s_2^2}{(s_1 - s_2) s_2} \right) \exp(s_2 t) + \frac{k_2}{s_1 s_2}, \qquad (11)$$

where s_1 and s_2 are the roots of the equation $G(s) = 0$, and

$$k_1 = \frac{V_{DD} + \omega_b R_c (V_{TL} C_x - e_v C_p)}{R_c (C_p + C_x)}, \qquad (12)$$

$$k_2 = \frac{V_{DD} \omega_b}{R_c (C_p + C_x)}. \qquad (13)$$

The ideal and actual exponential waveform of v_p (described by equations (7) and (11) respectively) are represented in figure 8 for $C_x = 100$ pF, $R_c = 100$ kΩ, $V_{DD} = 5$ V, $V_{TL} = V_{DD}/3$, $V_{TH} = 2V_{DD}/3$, $f_b = 500$ kHz and $C_p = 100$ pF. Except for the value of f_b, which is small so its effects can be seen more clearly, the rest of the values are usual. Figure 8 shows that, due to the limited bandwidth of the OpAmp and the effect of C_p, the transient response is slower and the charging time is longer. As a result, there is an error in the charging time.

Equation (11) does not have a symbolical solution for t_{ch}. Consequently, the actual value of t_{ch} and its relative error (using the value provided by (8) as a reference value) have
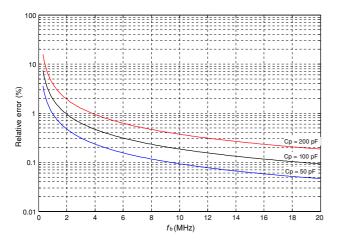
Figure 9. Relative error in the charging time as caused by the limited bandwidth of the OpAmp and the parasitic capacitance of the coaxial cable.

Figure 10. Experimental setup used to test the stability of active shielding.

Table 1. Nominal and measured unity-gain bandwidths (f_b) of the tested OpAmps.

OpAmp	Nominal f_b (MHz)	Actual f_b (MHz)
OPA344	1	1.2
OPA337	3	3.6
OPA743	7	5.4
TLC071	10	11
AD8655	28	30
OPA350	38	64

been calculated numerically. Figure 9 shows the relative error of t_{ch} versus f_b for different values of C_p (50 pF, 100 pF and 200 pF, which correspond to 0.5 m, 1 m and 2 m of cable length respectively) when $C_x = 100$ pF, $R_c = 100$ kΩ, $V_{DD} = 5$ V, $V_{TL} = V_{DD}/3$ and $V_{TH} = 2V_{DD}/3$. From figure 9, we can conclude that, whenever the circuit is stable, the greater the value of f_b or the shorter the length of the coaxial cable, the smaller the relative error in the charging time.

If the oscillator has symmetrical threshold voltages with respect to $V_{DD}/2$, the charging and discharging times are the same length. In addition, the time errors as caused by active shielding are equal for both time intervals. Consequently, the results shown in figure 9 can also be applied to estimate the overall relative error for the whole period of the oscillator output signal. For instance, for $\ell = 1$ m and $f_b = 10$ MHz, the period of the output signal has a relative error of 0.2%.

An error in the period of the oscillator output signal directly brings about an error in the estimation of C_x and, hence, in the estimation of the measurand. Auto-calibration methods, such as the three-signal technique [16], cannot compensate for this error because the reference components, which, in a practical setup, are built together with the interface circuit, do not suffer from the influence of active shielding. Therefore, it is advisable to reduce this error by selecting an OpAmp with a large f_b value. However, at the same time, the circuit must be stable and, hence, $f_b < f_{stab}$ (figure 7). Consequently, there is an optimal range of f_b values that provide both stability and accuracy.

4. Experimental results

The performance of active shielding was experimentally tested in terms of stability and accuracy. To evaluate the effect of the bandwidth of the OpAmp, we selected six commercial OpAmps with different bandwidths. All of these OpAmps can operate at a single supply voltage and fulfil the requirements listed in section 2. Table 1 lists the OpAmps and their nominal and actual f_b values. The actual value was measured using a sinusoidal frequency sweep. Except for OPA743, the actual value of f_b was always higher than the nominal one.
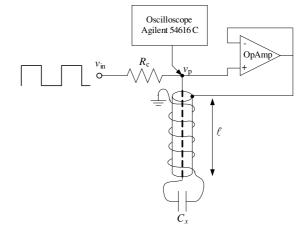
4.1. Stability

Figure 10 shows the experimental setup used to test the stability. A square-wave signal, which is the input of the circuit under normal operating conditions, was connected to v_{in}. To display the potential instability of the circuit, the signal v_p was monitored by a digital oscilloscope (Agilent 54616C) via a 10× probe (with 10 MΩ||9 pF input impedance). The circuit was considered unstable when a non-decreasing oscillation was superimposed on the exponential signal. The interconnection between the circuit and C_x was implemented using coaxial cable for the signal path and one-wire cable for the return path. The one-wire cable was twisted along the coaxial cable in order to reduce the area of the current loop. The features of this interconnection cable were characterized using an impedance analyser (Agilent 4294A), and the results were $r_p = 1.0$ Ω m^{-1}, $c_p = 100$ pF m^{-1} and $l_p = 1.0$ μH m^{-1}. The value of the resistor R_c was 100 kΩ.

First, in order to validate the circuit model of the interconnection cable shown in figure 4(*b*), we tested the stability of, on the one hand, the circuit in figure 4(*a*) for $\ell = 5$ m and, on the other hand, the circuit in figure 4(*b*) for $R_p = 4.7$ Ω, $C_p = 470$ pF and $L_p = 5$ μH, which are approximately the parasitic components of a 5 m interconnection cable according to our model. Both circuits became unstable under the same test conditions. This means that the circuit model seems to be accurate enough to evaluate the stability of the circuit.

We tested the stability for several values of C_x (10 pF, 47 pF, 100 pF and 470 pF, which were emulated by means of ceramic capacitors), ℓ (0 m, 0.5 m, 1 m and 5 m) and f_b

Table 2. Experimental results of the stability tests.

| OpAmp | Experimental instability cases | | |
	$\ell = 0.5$ m	$\ell = 1$ m	$\ell = 5$ m
OPA344	Stable	Stable	Stable
OPA337	Stable	Stable	Stable
OPA743	Stable	Stable	Stable
TLC071	Stable	$C_x \geqslant 470$ pF	$C_x \geqslant 100$ pF
AD8655	$C_x \geqslant 470$ pF	$C_x \geqslant 100$ pF	$C_x \geqslant 47$ pF
OPA350	$C_x \geqslant 47$ pF	$C_x \geqslant 47$ pF	$C_x \geqslant 47$ pF

(those listed in table 1). Table 2 summarizes the experimental results. For OPA344 and OPA337, the circuit was always stable. This is in agreement with figure 7, because when $\ell \leqslant 5$ m and $C_x \leqslant 470$ pF, the critical frequency f_{stab} is always greater than the bandwidth of these OpAmps. For TLC071 and OPA350, the circuit was unstable under certain conditions (see table 2), which is also predictable from figure 7 for $f_b = 11$ MHz and $f_b = 64$ MHz, respectively. However, for the other two OpAmps, some experimental results disagree with the theoretical predictions depicted in figure 7. For OPA743, the circuit should be unstable when $\ell = 5$ m and $C_x = 470$ pF, but experimentally it was stable. For AD8655, in addition to the cases listed in table 2, the circuit should also be unstable for (a) $\ell = 0.5$ m and $C_x = 100$ pF, and (b) $\ell = 1$ m and $C_x = 47$ pF. These disagreements may be due to an OpAmp output resistance higher than 50 Ω, which is assumed in figure 7 (see section 3.1). If the actual value of R_o is higher than 50 Ω, then the circuit can be stable under conditions in which, according to figure 7, it should be unstable.

Finally, we improved the stability of the circuit by connecting a 100 Ω resistor in series with the OpAmp output. Using this resistor, we had fewer instability cases, as predicted in section 3.1. For example, for TLC071, the circuit was unstable only when $\ell \geqslant 5$ m and $C_x \geqslant 470$ pF. Regrettably, this additional resistor increases the effective output impedance of the OpAmp and, hence, can worsen the rejection of external interference, especially at high frequencies.

4.2. Accuracy

Figure 11 shows the experimental setup used to evaluate the error in the measurement of C_x as caused by active shielding. A comparator-based relaxation oscillator was used as an interface circuit [11] and its output signal period was measured by a universal counter (Agilent 53131A). To avoid/reduce errors due to the non-idealities of the comparator, we used a high-speed comparator (TLV3501, 4.5 ns propagation delay) with a rail-to-rail output. We selected $R_1 = R_2 = R_3$ ($= 10$ kΩ), so that $V_{\text{TL}} = V_{\text{DD}}/3$ and $V_{\text{TH}} = 2V_{\text{DD}}/3$, and hence the duty cycle of the output signal was 50%. Other component values were $C_x = 100$ pF, $R_c = 100$ kΩ and $V_{\text{DD}} = 5$ V.

First, a capacitor C_p was used instead of the interconnection cable, as shown in figure 11. The period of the oscillator output signal was measured for the six OpAmps listed in table 1 and for three values of C_p (0 pF, i.e. without any capacitor, 100 pF and 200 pF). The case $C_p = 0$ pF was used as a reference to calculate the relative error of the period. Table 3 summarizes the resultant relative errors. On the one hand, the error for $C_p = 200$ pF was approximately twice that
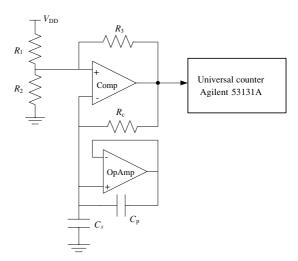

Figure 11. Experimental setup used to analyse the error in the measurement of C_x as caused by active shielding.

Table 3. Experimental results of the accuracy tests.

| OpAmp | Experimental relative error (%) | |
	$C_p = 100$ pF	$C_p = 200$ pF
OPA344	1.53	3.21
OPA337	0.58	1.09
OPA743	0.39	0.62
TLC071	0.24	0.44
AD8655	0.14	0.24
OPA350	0.11	0.19

for $C_p = 100$ pF, and, on the other hand, the error clearly decreased when the bandwidth of the amplifier increased. This performance agrees with the theoretical results shown in figure 9. Quantitatively, the experimental relative errors were slightly greater than the theoretical ones.

Finally, we measured the error in the period of the output signal when C_x was connected to the interface circuit via a 1 m interconnection cable. For OPA344, OPA337, OPA743 and TLC071, the resulting errors were very similar to those shown in table 3 for the case $C_p = 100$ pF, as expected since $c_p = 100$ pF m^{-1}. However, for AD8655 and OPA350, the error could not be measured because the circuit became unstable under such conditions, as indicated in section 4.1 as well. Therefore, the model developed in section 3.2 is helpful in predicting the error caused by active shielding whenever the circuit fulfils the stability condition described by equation (5).

5. Conclusions

The design of active shielding for grounded capacitive sensors requires special attention in order to prevent instability and inaccuracy. As the length of the shielded cable increases, so do the instability and the inaccuracy. However, an appropriate selection of the bandwidth of the amplifier that drives the shield of the coaxial cable can overcome these limitations. On the one hand, a wide bandwidth improves accuracy, but, on the other hand, a narrow bandwidth improves stability. Therefore, there is an optimal bandwidth range in terms of stability and accuracy. This is especially of interest

for measurement systems intended for large/medium-value capacitive sensors. For low-value capacitive sensors (say, below 10 pF), no instability problems are expected since the critical frequency f_{stab} is very high, and hence we can use a wide-bandwidth amplifier. Additional analysis is required for big-size capacitive sensors, such as liquid-level sensors for rivers or containers, since their parasitic components can also play an important role in the stability of the circuit.

Acknowledgments

References

[1] Baxter L K 1997 *Capacitive Sensors. Design and Applications* (New York: IEEE)

[2] Ross P J 1983 A water-level sensor using a capacitance to frequency converter *J. Phys. E: Sci. Instrum.* **16** 827–8

[3] Bera S C, Ray J K and Chattopadhyay S 2006 A low-cost noncontact capacitance-type level transducer for a conducting liquid *IEEE Trans. Instrum. Meas.* **55** 778–86

[4] Haase W C 2004 Digital measurement circuit and system using a grounded capacitive sensor *US Patent Specification* 6,700,392

[5] Herzog M 1988 Circuit for measuring capacitance by charging and discharging capacitor under test and its shield *US Patent Specification* 4,743,837

[6] Huang S M, Stott A L, Green R G and Beck M S 1988 Electronic transducers for industrial measurement of low value capacitances *J. Phys. E: Sci. Instrum.* **21** 242–50

[7] Marioli D, Sardini E and Taroni A 1993 High-accuracy measurement techniques for capacitance transducers *Meas. Sci. Technol.* **4** 337–43

[8] Rich A 1983 Shielding and guarding *Application Note AN-347* Analog Devices

[9] Morrison R 1995 *Solving Interference Problems in Electronics* (New York: Wiley)

[10] Pallas-Areny R and Webster J G 2001 *Sensors and Signal Conditioning* 2nd edn (New York: Wiley)

[11] Qi J, Meijer G C M, Li X and Guan C 2005 An integrated interface for grounded capacitive sensors *Proc. 4th IEEE Sensors Conf. (Irvine, CA, USA)*

[12] Franco S 2002 *Design with Operational Amplifiers and Analog Integrated Circuits* 3rd edn (New York: McGraw-Hill)

[13] Dorf R C and Bishop R H 2005 *Modern Control Systems* 10th edn (Upper Saddle River, NJ: Pearson–Prentice Hall)

[14] Mancini R 2001 *Op Amps for Everyone. Design Reference* Texas Instruments

[15] Goedbloed J J 1992 *Electromagnetic Compatibility* (New York: Prentice Hall)

[16] Meijer G C M, Van der Goes F M L, De Jong P C, Li X and Toth F N 1999 Integrated interfaces for low-cost multiple-sensor systems *J. Intell. Mater. Syst. Struct.* **10** 105–15